Residual stress modeling in minimum quantity lubrication grinding

Yamin Shao[1] · Omar Fergani[2] · Beizhi Li[3] · Steven Y. Liang[1]

Abstract Minimum quantity lubrication (MQL) has been proposed as a promising alternative to conventional flood cooling to substantially reduce the lubrication usage while maintaining high surface quality. Residual stress induced by grinding process directly affects the surface quality of the final product. An analytical relationship between residual stresses and process conditions such as process parameters, material properties, and lubrication conditions could support process planning and optimization of MQL grinding. This paper has presented a physics-based model to predict residual stresses in grinding with consideration of the lubrication and cooling effects of MQL. Grinding force and temperature distribution in the workpiece are used to calculate the loading stresses imparted by MQL grinding. The loading stresses are then coupled into a rolling/sliding contact algorithm to solve for residual stresses. Experimental measurements of residual stress profile under and flood cooling conditions have been pursued to calibrate and validate the predicted results.

Keywords Residual stress · Analytical modeling · Minimum quantity lubrication · Grinding

✉ Yamin Shao
  ymshao@gatech.edu

1 George W. Woodruff School of Mechanical Engineering, Georgia Institute of Technology, 813 Ferst Dr. Rm. 458, Atlanta, GA 30332-0560, USA

2 Schlumberger Company, 23500 Colonial Pkwy, Katy, TX 77493, USA

3 College of Mechanical Engineering, Donghua University, 2999 North Renmin Rd., Songjiang District, Shanghai, China 201620

1 Introduction

In recent years, the sustainability of the manufacturing processes has gained increasing attention. The pressure from public authorities has driven the researchers to seek alternative production processes, creating technologies that can reduce cost and conserve energy. In the last two decades, the research focus has been set to greatly reduce the use of cooling/lubricating fluids in metalworking processes [1]. In grinding process, while completely eliminating the use of fluid can cause problems like high wheel wear, limited material removal rate, workpiece thermal damage, clogging of the wheel, and loss of dimensional and geometrical precision of the workpiece, minimum quantity lubrication appears to be a promising alternative to overcome these problems.

In assessing the process performance, residual stress plays an important role for its effects on the fatigue life, corrosion resistance, and part distortion. Since grinding is usually one of the final operations of the technological process, properties of surface layer created directly influence the functionality of the workpiece. The functional behavior of components can be enhanced or impaired by residual stresses. Therefore, evaluation of the residual stress imparted by minimum quantity lubrication (MQL) grinding is critical to understand the process.

Investigation of residual stresses in grinding operation has been an interest to researchers for several decades. Empirical, finite element analysis (FEA) and analytical approach has been proposed in these investigations. Kruszynski and Wojcik [2] developed an empirical model for predicting residual stress in grinding by relating the residual stress to a coefficient B which is a product of power density and contact time. Mahdi and Zhang [3] have studied the full coupling of mechanical deformation, thermal deformation, and phase transformation during grinding using finite element method. Chen et al. [4] have investigated the tensile residual stress caused by

Springer

thermal expansion and contraction. A critical transitional temperature from compressive to tensile residual stress has been determined for En9 steel. The authors [5] developed an analytical model to predict the thermally induced residual stress in grinding process and predicted the transitional temperature for AISI 52100 steel. Regarding the application of MQL, it has been widely studied in machining processes [6, 7]. However, MQL grinding is still a relatively new topic and the documented researches have been majorly experimental observations. Silva et al. [8] has compared MQL grinding to dry and wet conditions in grinding 4340 steel with aluminum oxide wheel. Their results showed MQL grinding achieved less surface roughness and more compressive residual stress on the ground surface than other conditions. Shen [9] studied the tribological properties and grinding performance of MQL grinding using nanofluids compared to pure water or oil MQL applications as well as dry and wet grinding. Tawakoli et al. [10] have investigated the influence of process parameters on MQL grinding performance in terms of force, surface roughness, surface morphology, grinding temperature, and energy partition. The authors [11] investigated the grinding performance in terms of grinding force, temperature, as well as residual stress behavior in MQL grinding process. Regarding analytical modeling effort, Hadad and Sadeghi [12] have proposed an analytical model to calculate the temperature distribution in the workpiece under MQL grinding. The authors [13, 14] have proposed a comprehensive model to calculate the grinding force, temperature, and surface roughness under MQL conditions from a physics-based approach.

Literature survey shows lack of analytical studies of residual stress behavior in MQL grinding process. This paper presented an analytical approach to predict the residual stresses in MQL grinding. The utilization of analytical models to predict residual stress is pursued due to the short computational time and accurate understanding of physical mechanisms. In this study, the effect of MQL on tribological properties and thermal properties are reflected in the force and temperature calculation. Mechanical and thermal loading stresses are calculated based on contact mechanics and thermoelasticity

theories. Using the stress fields captured from the forces, contact zones, and thermal predictions, the residual stresses are computed from a rolling/sliding contact algorithm developed by McDowell [15]. The proposed residual stress prediction model is calibrated and validated by surface grinding of AISI 1018 steel with aluminum oxide wheel.

2 Modeling approach

The MQL fluid provides lubricating and cooling in the grinding process. For the lubrication effect, it changes the tribological behavior at the grit-workpiece interface and alters the contact stress in grinding. For the cooling effect, it affects the temperature distribution in the workpiece and thus the thermal stress. The mechanical and thermal stresses are captured, subsequently, in an elastic-plastic model to calculate the resulting residual stress profile. A flowchart of residual stress modeling in MQL grinding is shown in Fig. 1. The process parameters, wheel characteristics, workpiece material properties, and lubrication conditions are taken as inputs to predict the residual stress.

3 Force modeling in MQL grinding

In the proposed model, the grinding force can be solved from a probabilistic approach based on single-grit interaction analysis and undeformed chip thickness distribution. The single-grit interaction mechanisms including chip formation, ploughing, and rubbing have been investigated. Details of the grinding force modeling are documented in the author's previous work [14]. Here, a short introduction is made for the modeling approach.

In MQL grinding, the lubrication effect is represented by boundary lubrication as lubricant film is only partially established due to the limited amount of lubricant. Boundary lubrication theory [16] is applied to describe the tribological behavior in MQL grinding. The most important two

Fig. 1 General residual stress modeling approach
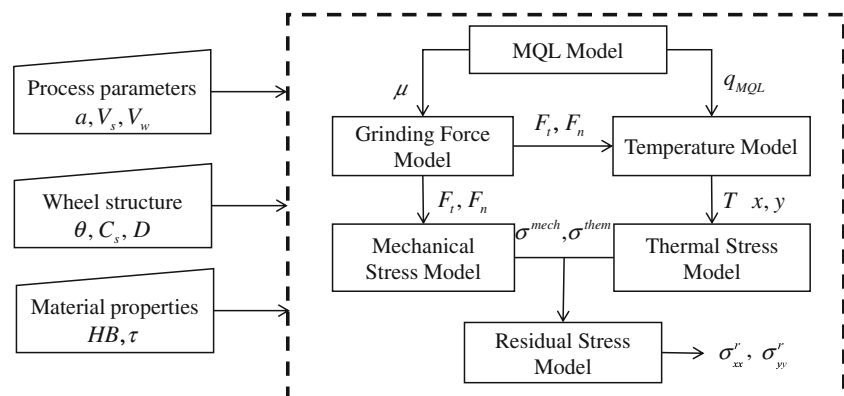
parameters need to be determined are the following: (a) the approach of two surfaces a_s, which can be solved from the cubic function (1); (b) the friction coefficient, which is calculated by Eq. (3).

$$a_s^3 + 3C_2 t_b a_s^2 + 3C_2 t_b^2 a_s + \left[C_2 t_b^3 - N/(p_m Q)\right] = 0 \qquad (1)$$

where

$$Q = \pi R n_0 D^2 / \left(6 H_{\max}^2\right) \qquad (2)$$

$$\mu = \frac{C_1 a_s^3 + C_2 C_3 \left\{(a_s + t_b)^3 - a_s^3\right\}}{a_s^3 + C_2 \left[(a_s + t_b)^3 - a_s^3\right]} \qquad (3)$$

Here, C_1, C_2, and C_3 are coefficients as related to lubrication conditions and coolant properties, while C_2 is assumed to be 0.5 in boundary lubrication. The N is the normal load, R is the asperity tip radius, n_0 is the total asperity number, D is the inclination distribution function, $H_{\max}$ is the asperity height distribution, and t_b is the effective adsorbed lubricant film thickness. In this study, the grit ship is assumed to be conical with a rounded tip and wear flat area. To model the single-grit force, three components are considered: chip formation force, ploughing force, and rubbing force [14] as shown in Fig. 2.

Due to the randomness of grit distribution on the wheel surface, grits will have different engagement depths in the grinding process. The grinding force calculation hinges upon the undeformed chip thickness distribution, which was described by a Rayleigh probability density function (p.d.f.) in this study.

$$f(t) = \begin{cases} \left(t/\sigma^2\right)\exp\left(-t^2/2\sigma^2\right) & t \geq 0 \\ 0 & t < 0 \end{cases} \qquad (4)$$

The parameter σ, that completely defines this p.d.f., was calculated as a function of the grinding wheel microstructure (grain shape, static grit density); dynamic effects (local grain deflection and wheel-workpiece contact deflection); and grinding conditions (wheel depth of cut, wheel and workpiece tangential velocity).
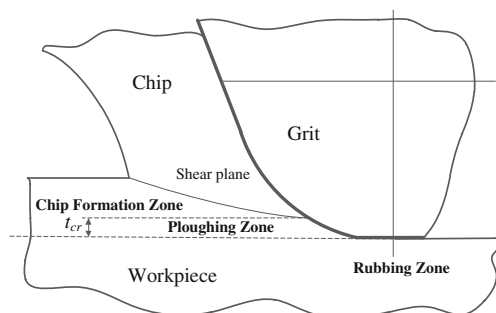

Fig. 2 Schematic of single-grit interaction

4 Thermal modeling in MQL grinding

In this study, a triangular moving heat source with a heat loss from MQL fluid is modeled as shown in Fig. 3. The solution for the moving heat source can be represented by Bessel functions and obtained by summing over the length of the contact zone. The temperature at any point (x, z) in the workpiece is given as [14]:

$$T_{(x,z)} = \int_{-l_c/2}^{l_c/2} (q_{\text{in}} - q_{\text{out}})/(\pi k_w)\exp(V_w(x-x')/(2\alpha_w)) \\ K_0\left\{V_w\left[(x-x')^2 + z^2\right]^{1/2}/(2\alpha_w)\right\} dx' \qquad (5)$$

where q_{in} is the total heat flux into the workpiece and fluid, q_{out} is the heat flux taken away by fluid, k_w is the thermal conductivity of the workpiece, α_w is the thermal diffusivity given by $\alpha_w = k_w/\rho_w c_w$, where ρ_w is the workpiece density, c_w is the workpiece-specific heat, and K_0 is the modified Bessel function of the second kind of order zero. The q_{in} and q_{out} are calculated based on energy partition and heat transfer analysis. The details of the thermal analysis can be found in the authors' previous work [14].

5 Residual stress modeling

In order to model residual stresses, the stress history experienced by the workpiece needs to be known. The causes for residual stresses in ground workpiece are majorly from mechanical deformation, thermal expansion, and contraction and material phase transformation [4]. The residual stress induced by phase transformation is ignored in this research assuming that the grinding zone temperature does not reach the phase transformation triggering temperature. The phase transformation can be indeed important factors on residual stress, on which the authors have begun to explore in other publications [17].

The mechanical-induced stress is due to localized interactions of abrasive grains with the workpiece. The workpiece is modeled as an isotropic, elasto-plastic material with a von Mises yield surface. The elastic modulus and the Poisson's ratio of the workpiece are E and ν, and the coefficient of
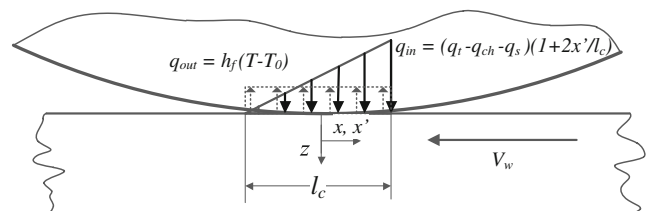

Fig. 3 Temperature modeling schematic

thermal expansion is α. Assuming a state of plain strain in y direction ($\varepsilon_{yy}=0$), at the local scale, the single-grit forces are modeled as distributed load with tangential pressure p(s) and normal pressure q(s) as shown in Fig. 4. Assuming the stress profiles are known, the stresses in the workpiece are computed by integrating the Boussinesq solution for normal and tangential point loads in semi-infinite bodies over the region of contact as given in Eq. (6).

$$
\begin{aligned}
\sigma_{xx}^{mech}(x,z) &= -(2z/\pi) \int_{-a}^{a} \left(p(s)(x-s)^2 ds \right) / \left((x-s)^2 + z^2 \right)^2 - (2/\pi) \int_{-a}^{a} \left(q(s)(x-s)^3 ds \right) / \left((x-s)^2 + z^2 \right)^2 \\
\sigma_{zz}^{mech}(x,z) &= -(2z^3/\pi) \int_{-a}^{a} (p(s)ds) / \left((x-s)^2 + z^2 \right)^2 - (2z^2/\pi) \int_{-a}^{a} (q(s)(x-s)ds) / \left((x-s)^2 + z^2 \right)^2 \\
\sigma_{xz}^{mech}(x,z) &= -(2z^2/\pi) \int_{-a}^{a} (p(s)(x-s)ds) / \left((x-s)^2 + z^2 \right)^2 - (2z/\pi) \int_{-a}^{a} \left(q(s)(x-s)^2 ds \right) / \left((x-s)^2 + z^2 \right)^2 \\
\sigma_{yy}^{mech}(x,z) &= \nu \left(\sigma_{xx}^{mech}(x,z) + \sigma_{zz}^{mech}(x,z) \right)
\end{aligned}
\tag{6}
$$

where the span of the integrals [−a, a] is a function of the grit tip radius, wear flat length, and undeformed chip thickness. To simplify the problem, the normal contact pressure due to the grit-workpiece interaction is assumed to be two-dimensional Hertzian. The maximum Hertzian pressure, p_0, due to the normal load of single grit, is shown in Eq. (7). The shear stress p_0 at the interface is assumed to be uniformly distributed and proportional to the tangential load of the single grit.

$$
p_0 = 3 F_{ng} / (2\pi a^2), \quad \tau = F_{tg} / (\pi a^2)
\tag{7}
$$

On the other hand, the thermally induced stress field due to non-uniform temperature distribution T are calculated based on the Timoshenko thermoelasticity theory [18]. He proposed a three-step approach to calculate the total thermal stresses by superposing the following components:

(a) Stresses due to body force $X=-(\alpha E/(1-2\nu))(\delta T/\delta x)$ and $Z=-(\alpha E/(1-2\nu))(\delta T/\delta z)$,
(b) Stresses due to a tensile surface traction of $\alpha ET/(1-2\nu)$,
(c) A hydrostatic pressure of $-\alpha ET/(1-2\nu)$.

The resulting thermal stress components are given in (8)

$$
\begin{aligned}
\sigma_{xx}^{therm}(x,z) &= -\frac{\alpha E}{1-2\nu} \int_0^\infty \int_{-\infty}^\infty \left(G_{xh} \frac{\partial T}{\partial x}(x',z') + G_{xv} \frac{\partial T}{\partial z}(x',z') \right) dx'dz' + \frac{2z}{\pi} \int_{-\infty}^\infty \frac{p(t)(t-x)^2}{\left((t-x)^2 + z^2 \right)^2} dt - \frac{\alpha E T(x,z)}{1-2\nu} \\
\sigma_{zz}^{therm}(x,z) &= -\frac{\alpha E}{1-2\nu} \int_0^\infty \int_{-\infty}^\infty \left(G_{zh} \frac{\partial T}{\partial x}(x',z') + G_{zv} \frac{\partial T}{\partial z}(x',z') \right) dx'dz' + \frac{2z^3}{\pi} \int_{-\infty}^\infty \frac{p(t)}{\left((t-x)^2 + z^2 \right)^2} dt - \frac{\alpha E T(x,z)}{1-2\nu} \\
\sigma_{xz}^{therm}(x,z) &= -\frac{\alpha E}{1-2\nu} \int_0^\infty \int_{-\infty}^\infty \left(G_{xzh} \frac{\partial T}{\partial x}(x',z') + G_{xzv} \frac{\partial T}{\partial z}(x',z') \right) dx'dz' + \frac{2z^2}{\pi} \int_{-\infty}^\infty \frac{p(t)(t-x)}{\left((t-x)^2 + z^2 \right)^2} dt \\
\sigma_{yy}^{therm}(x,z) &= \nu \left(\sigma_{xx}^{therm} + \sigma_{zz}^{therm} \right) - \alpha E T(x,z)
\end{aligned}
\tag{8}
$$

where

$$
p(t) = \frac{\alpha E T(x, z=0)}{1-2\nu}
\tag{9}
$$

and (G_{xh}, G_{zh}, G_{xzh}, G_{xv}, G_{zv}, G_{xzv}) are the plain strain Green's functions as can be found in the literature [19].

The stress history experienced by the workpiece due to combined effect of mechanical and thermal stress is further discussed here. The grit is travelling at a much higher speed (V_w+V_s) than the moving speed of wheel-workpiece contact zone V_w. In other words, during the time that the contact zone travels a certain length, many loading passes of the single-grit
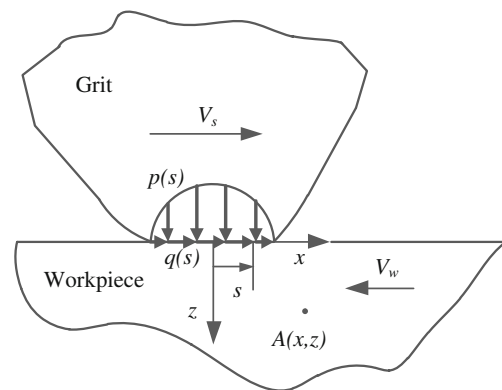

Fig. 4 Stress resulting from single-grit interaction at grit scale

interactions have been experienced by the workpiece. Therefore, the residual stress induced by mechanical deformation should be modeled as multiple loading passes. That is, the stresses and strains of the first pass are calculated and assigned to be the initial values for the next passage of the load. Although it is possible that the second grit will start to engage with the workpiece before the first grit disengage with the workpiece, it is still valid to make this assumption since the length scale of local stress field created by single-grit interaction is much smaller comparing to the distance between successive grits. The number of loading passes n_{pass} is determined by the contact length l_c, the average distance between active grits l_0, and the speed ratio $(V_w+V_s)/V_w$.

$$n_{pass} = (l_c/l_0)((V_w + V_s)/V_w) \tag{10}$$

Different form the mechanical loading, the thermal stress field is modeled from a larger scale considering the total heat input from all the grits in the wheel/workpiece contact zone. Therefore, the temperature field is moving at the speed of V_w and the stress history due to thermal stress field are obtained for a single loading pass. This model assumes that every location at a specified depth in the workpiece experiences the same thermo-mechanical loading history. Using the stress fields captured from both mechanical and thermal components, the residual stresses can be predicted based on plasticity models.

Here, a hybrid algorithm developed by McDowell [15] is adapted and utilized to compute the residual stresses. The model provides a robust, stable prediction of subsurface plasticity and residual stresses over a wide range of loading conditions. This algorithm uses a blending function Ψ, which is dependent on the instantaneous value of the modulus ratio h/G, where h is the plastic modulus, G is the elastic shear modulus, and κ is an algorithm constant. The blending function is given as:

$$\Psi = 1 - \exp(-\kappa(3h/2G)) \tag{11}$$

A cyclic plasticity framework is employed here, based on a von Mises yield surface as given in Eq. (12):

$$F = 3/2(s_{ij} - \alpha_{ij})(s_{ij} - \alpha_{ij}) - R^2 = 0 \tag{12}$$

where $s_{ij} = \sigma_{ij} - (\sigma_{kk}/3)\delta_{ij}$ is the deviatoric stress, α_{ij} is the back stress, and R is the uniaxial normalized radius of the yield surface. Johnson-Cook material constitutive model is used to capture the yield surface change due to thermal and strain rate effect.

The normality flow rule is used to calculate plastic strain increments:

$$\dot{\varepsilon}_{ij}^p = (1/h)\langle \dot{s}_{mn} n_{mn} \rangle n_{ij} \tag{13}$$

with $n_{ij} = \sqrt{(3/2)}(s_{ij} - \alpha_{ij})/R$, $\langle \rangle$ is the MacCauley bracket

defined as $\langle x \rangle = 0.5(x + |x|)$. Linear kinematic hardening is utilized in the model and the evolution of the back stress is given by:

$$\dot{\alpha}_{ij} = \langle \dot{s}_{mn} n_{mn} \rangle n_{ij} \tag{14}$$

For elastic-plastic loading, the blending function is used to describe the strain increment in the grinding direction as shown in Eq. (15). Similarly, the plane-strain condition is imposed as given in Eq. (16). The quantities superscripted with asterisks represent the elastic solution.

$$\begin{aligned} \dot{\varepsilon}_{xx} &= \frac{1}{E}\left[\dot{\sigma}_{xx} - \nu\left(\dot{\sigma}_{yy} + \dot{\sigma}_{zz}^*\right)\right] + \frac{1}{h}\left(\dot{\sigma}_{xx}n_{xx} + \dot{\sigma}_{yy}n_{yy} + \dot{\sigma}_{zz}^*n_{zz} + 2\dot{\tau}_{xz}^*n_{xz}\right)n_{xx} \\ &= \Psi\left(\frac{1}{E}\left[\dot{\sigma}_{xx}^* - \nu\left(\dot{\sigma}_{yy} + \dot{\sigma}_{zz}^*\right)\right] + \frac{1}{h}\left(\dot{\sigma}_{xx}^*n_{xx} + \dot{\sigma}_{yy}n_{yy} + \dot{\sigma}_{zz}^*n_{zz} + 2\dot{\tau}_{xz}^*n_{xz}\right)n_{xx}\right) \end{aligned} \tag{15}$$

$$\begin{aligned} \dot{\varepsilon}_{yy} &= \frac{1}{E}\left[\dot{\sigma}_{yy} - \nu\left(\dot{\sigma}_{xx} + \dot{\sigma}_{zz}^*\right)\right] \\ &+ \frac{1}{h}\left(\dot{\sigma}_{xx}n_{xx} + \dot{\sigma}_{yy}n_{yy} + \dot{\sigma}_{zz}^*n_{zz} + 2\dot{\tau}_{xz}^*n_{xz}\right)n_{yy} = 0 \end{aligned} \tag{16}$$

The equations are solved simultaneously to determine the increments of stress for $\dot{\sigma}_{xx}$ and $\dot{\sigma}_{yy}$. The stress increments are integrated over the passage of the load to determine the residual stresses. At the end of each pass, the stresses are relaxed [15] to satisfy boundary conditions. The residual stresses are calculated as a superposition of mechanical and thermal loading stresses due to their difference in the scale of influenced area, strain rate, and cyclic/non-cyclic loading characteristics. For modeling, the mechanical-induced residual stress, the routine is repeated for the number of passes in Eq, (10) with the previous residual stresses assigned to be the initial values for the next passage of the load. The thermal-induced residual stress is calculated from one loading passage as mentioned above.

6 Experimental validation

The experiments were performed on the Bridgeport GX 480 Vertical Milling center in order to validate the predictive models. The CNC milling center was used instead of the grinding machine for the following reasons: (1) simple set up of the measurement equipment, (2) precise control of spindle rotational speed up to 10,000 RPM, and (3) a positional

Table 1   Thermal properties of AISI 1018 steel and Al$_2$O$_3$ wheel [14]

Material	Thermal conductivity (W/m K)	Density (kg/m^3)	Specific heat (J/kg K)	Thermal diffusivity (m^2/s)
AISI 1018	51.9	7870	486	1.36e-5
Al$_2$O$_3$	46	3970	765	1.52e-5

Table 2 Thermal properties of air and vegetable oil at room temperature [14]

Material	Thermal conductivity (W/m K)	Density (kg/m³)	Specific heat (J/kg K)	Dynamic viscosity (Pa s)
Air	0.026	1.16	1007	1.8e-5
Vegetable oil	0.17	980	1675	38.63e-3
Air-oil mixture	0.027	1.24	1035	1.92e-5

accuracy of 0.00254 mm. Each test was repeated twice to ensure accuracy of the results. The MQL supply system was Coolubricator™ manufactured by UNIST, Inc. with the lubrication medium of vegetable oil and flow rate of 396 ml/h. The pressurized air pressure was supplied externally at four bars. The distance from the nozzle to the contact zone was 40 mm and the impingement angle is 10 °. The grinding wheel employed in this study was vitrified-bonded aluminum oxide wheel (Norton 38A120-KVBE). The wheel speed was kept at 23.92 m/s. The wheel was dressed by a single-point diamond dresser before every test. The dressing depth is 16 μm and overlap ratio is 1.68. Surface grinding tests were carried out with a single pass of 150-mm length on the AISI 1018 steel workpiece with 9.5-mm width. The reason for not doing multiple passes experiment is that the residual stresses generated from previous passes may influence the result of current pass. The surface to be ground is achieved by several pre-test grinding steps. These grinding steps are carried at extremely low material removal rate (specific MRR=2.15e-3 mm²/s) to avoid introducing large subsurface residual stress to the workpiece. It is assumed that the residual stress affected depth due to pre-test grinding steps is very small and will be removed by the experimental grinding pass. The thermal properties of the workpiece, wheel, and MQL fluid are listed in Tables 1 and 2. The Johnson-Cook parameters for AISI 1018 steel are listed in Table 3.

The grinding forces were recorded using a piezo-electric transducer-based dynamometer (type Kistler 9257B). Temperature history in the workpiece at a certain depth was recorded using Omega type K thermocouple and Omega OM-DAQ-USB-2401 data acquisition system with a sampling frequency of 100 Hz. The residual stresses in tangential and traverse direction were measured on PROTO LXRD 2000 x-ray diffraction machine. The source is 3 kW ceramic/metal Model XRT 60 x-ray tube with Cr anode and the detector is proprietary dual position-sensitive scintillation detectors (PSSD). The measurement was taken with seven psi tilt angles

**Table 3** AISI 1018 steel Johnson-Cook parameters [20]

Material	A (MPa)	B (MPa)	n	C	m
AISI 1018	520	269	0.282	0.0476	0.553

Table 4 Process parameters and lubrication conditions

Lubrication	MQL			Wet		
Condition	1	2	3	1	2	3
Depth of cut (μm)	15.24	15.24	7.62	15.24	15.24	7.62
Feed rate (m/min)	1.524	0.762	1.524	1.524	0.762	1.524
Specific MRR (mm²/s)	0.387	0.194	0.194	0.387	0.194	0.194

from −20 to 20 °. PROTO Electropolisher Model 8818-V3 is used to remove layers from the specimen to expose the subsurface for residual stress measurement without incurring cold-working stresses. The input voltage, current, electrolyte, and polishing time was tested and adjusted to ensure constant polishing depth. Residual stress under maximum depth of 0.5 mm below the surface was measured with a step size of 0.1 mm.

In order to compare the effects of lubrication type, six sets are divided into two groups: MQL, and conventional flood cooling (represented as "wet" condition). For each group, three different process conditions are performed. The process parameters and lubrication conditions are summarized in Table 4.

(a)

(b)
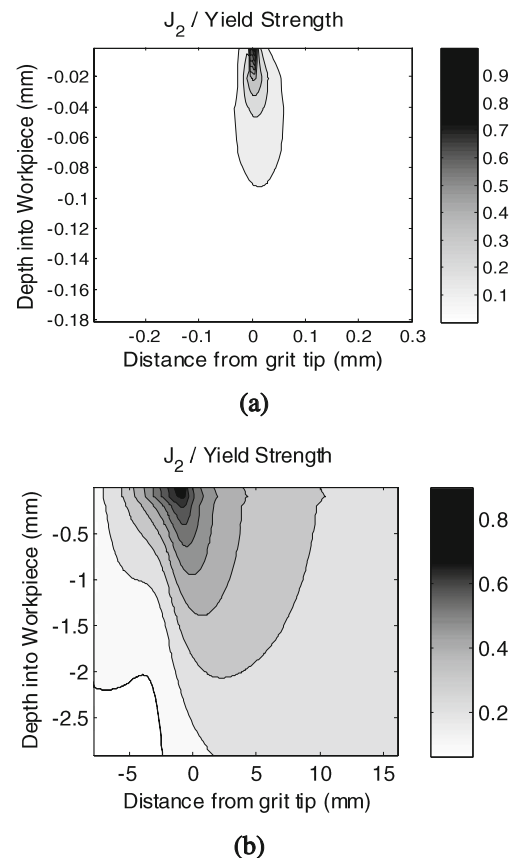
Fig. 5 Mechanical and thermal stress field

7 Results and discussion

The mechanical loading stress by an individual grit is calculated using Eq. (6) based on the single-grit force calculations. An example is given in Fig. 5 under condition 1 with MQL lubrication. It is discovered that plastic deformation induced by grit interactions only happen at the place very close to the surface (<0.1 mm) as shown from the calculated single-grit stress field in (Fig. 5a). In comparison, the thermal stress in the same condition is calculated using Eq. (8) based on the temperature distribution in the workpiece. The thermal loading stress is reaching to a larger depth underneath the surface. It can be concluded that for residual stresses in depth below the surface (>0.1 mm), the influence only come from the thermal stresses as shown in (Fig. 5b).

With the mechanical and thermal loading stress calculated, the residual stresses can be predicted based on McDowell algorithm. As suggested above, the mechanical effect is significant at the surface region while the thermal effect is reaching to a larger depth. The comparison between predicted and measured residual stress profiles are shown in Fig. 6.

It can be seen from the comparison that prediction results agree with experimental measurements reasonably well in both MQL and flood cooling situations. The difference between the experimental measurements and model predictions may come from the assumptions and simplifications used in the calculation of mechanical and thermal loading stresses. Several remarks are made here:

(a) Surface residual stresses in MQL and flood cooling conditions are compressive in the studied circumstances. The reason is that mechanical stress on the workpiece surface took the dominant position under these conditions while the surface temperature is not very high. It is suggested in previous studies [4] that a critical temperature exists for the transition from compressive to tensile surface residual stress. When the surface temperature exceeds the critical point, tensile residual stress will be generated on the workpiece surface. Due to the fact that MQL generates much higher surface temperature [14] under same grinding parameters, it is expected that lower material removal rate is

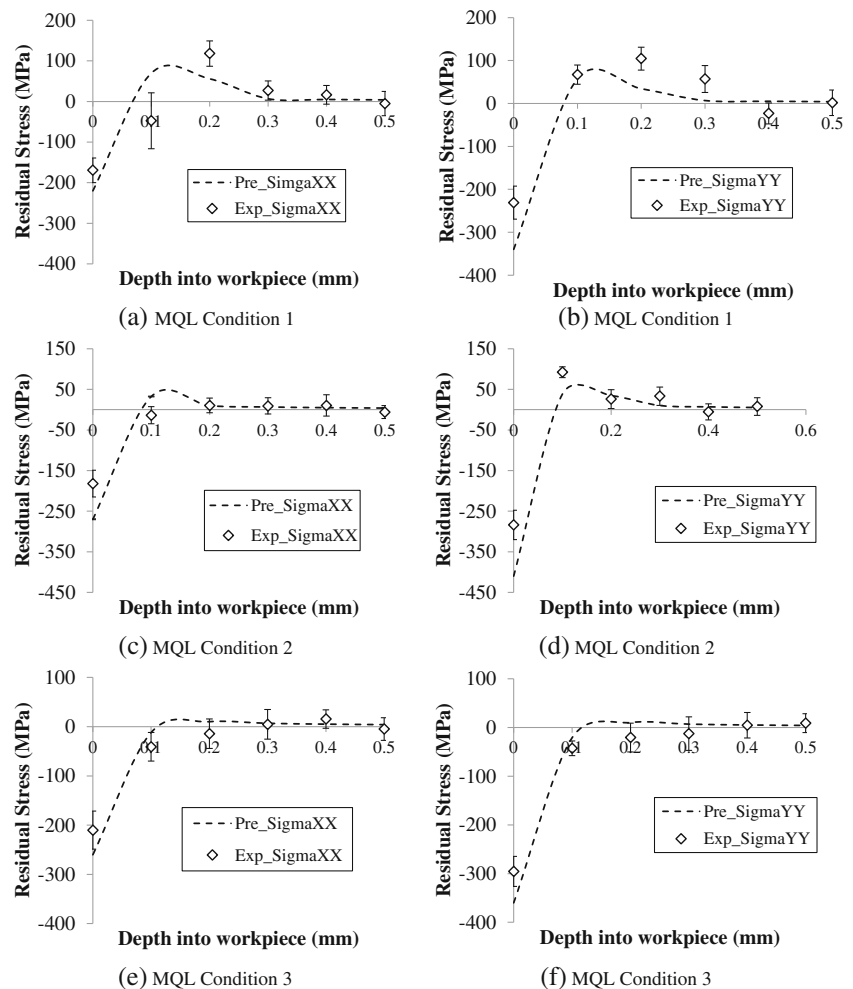Fig. 6 Comparison of residual stresses in experiment and simulation
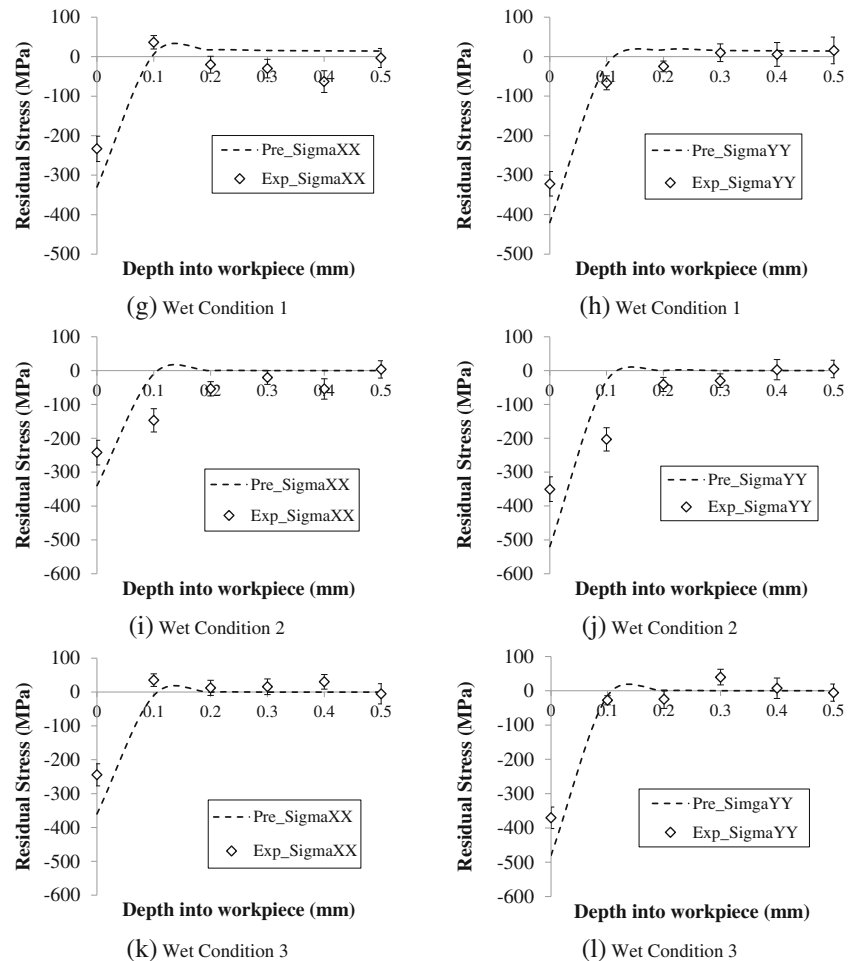
(a) MQL Condition 1

(b) MQL Condition 1

(c) MQL Condition 2

(d) MQL Condition 2

(e) MQL Condition 3

(f) MQL Condition 3

Fig. 6 (continued)

(g) Wet Condition 1

(h) Wet Condition 1

(i) Wet Condition 2

(j) Wet Condition 2

(k) Wet Condition 3

(l) Wet Condition 3

needed to reach transitional temperature for MQL grinding comparing to flood cooling. This is indicated in this study by that the residual stresses are more "tensile" in MQL condition which represents the thermal effect on the surface residual stress.

(b) Tensile stresses were generated in the subsurface area under conditions 1 and 2 in MQL grinding but not found in other conditions. The reason is that thermally induced stress could affect deeper subsurface areas while the mechanical stress affected areas are localized and very close to the surface. Since the temperature effect is negligible in other conditions, tensile residual stress are almost eliminated in the subsurface areas.

(c) The larger material removal rate in condition 1 results in a larger grinding energy and temperature under MQL condition. Consequently, the residual stresses are more tensile in condition 1 compared to conditions 2 and 3. However, the effect of large-material removal rate under flood cooling condition is not obvious since the temperature is not high enough to induce large thermal stresses.

8 Conclusions

A model for predicting residual stresses in grinding process under MQL condition has been presented in this paper. The grinding force and temperature distribution in the workpiece are first calculated considering MQL lubrication and cooling effect. Followed by the mechanical and thermal loading stress field captured based on grinding force and temperature calculations. The stresses are then coupled into an elastic-plastic contact algorithm to calculate the residual stresses.

The surface grinding of AISI 1018 steel experiments are used to validate the proposed prediction model. Due to the change in tribological and thermal properties induced by MQL, the residual stress profile could vary significantly from the flood cooling condition. It is found that the higher temperature generated in MQL grinding tend to shift the residual stress profile to the tensile direction. The result shows clearly the effect of mechanical and thermal stress on and below the workpiece surface.

This work offers theoretical insight of the MQL performance in the context of a key surface integrity factor—residual stress. It can be applied to a range of different grinding

conditions and materials and does not require extensive cali-bration in order to function. The model incorporates process conditions, material properties, wheel characteristics, and lu-brication conditions into a predictive model for grinding in-duced residual stresses.

The current residual stress considers only mechanical and thermal effects. However, the high temperature generated in the contact zone may lead to phase transformation that will induce additional residual stresses. Future investigation is needed to include the phase transformation mechanism to re-fine the residual stress model.

References

1. Autret R, Liang S (2003) Minimum quantity lubrication in finish hard turning. Proceedings of International Conference on Humanoid, Nanotechnology, Information Technology, Communication and Control, Environment, and Management, Manila

2. Kruszynski B, Wojcik R (2001) Residual stress in grinding. J Mater Process Technol 109(3):254–257. doi:10.1016/S0924-0136(00)00807-4

3. Mahdi M, Zhang L (1999) Applied mechanics in grinding. Part 7: residual stresses induced by the full coupling of mechanical defor-mation, thermal deformation and phase transformation. Int J Mach Tools Manuf 39(8):1285–1298. doi:10.1016/S0890-6955(98)00094-7

4. Chen X, Rowe W, McCormack D (2000) Analysis of the transition-al temperature for tensile residual stress in grinding. J Mater Process Technol 107(1–3):216–221. doi:10.1016/S0924-0136(00)00692-0

5. Fergani O, Shao Y, Lazoglu I, Liang S (2014) Temperature effects on grinding residual stress. Procedia CIRP 14:2–6. doi:10.1016/j.procir.2014.03.100

6. Ji X, Zhang X, Li B, Liang S (2014) Modeling of the effects of minimum quantity lubrication on machining force, temperature, and residual stress. Mach Sci Technol 18(4):547–564. doi:10.1080/10910344.2014.955367

7. Tai B, Stephenson D, Shih A (2013) Workpiece temperature during deep-hole drilling of cast iron using high air pressure minimum quantity lubrication. J Manuf Sci Eng 135(3):1–7. doi:10.1115/1.4024036

8. Silva L, Bianchi E, Fusse R, Catai R, Franca T, Aguiar P (2007) Analysis of surface integrity for minimum quantity lubricant—MQL grinding. Int J Mach Tools Manuf 47(2):412–418. doi:10.1016/j.ijmachtools.2006.03.015

9. Shen B, Shih A, Tung S (2008) Application of nanofluids in min-imum quantity lubrication grinding. Tribol Trans 51(6):730–737. doi:10.1080/10402000802071277

10. Tawakoli T, Hadad M, Sadeghi M, Daneshi A, Stockert S, Rasifard A (2009) An experimental investigation of the effects of workpiece and grinding parameters on minimum quantity lubrication—MQL grinding. Int J Mach Tools Manuf 49(12–13):924–932. doi:10.1016/j.ijmachtools.2009.06.015

11. Shao Y, Fergani O, Ding Z, Li B, Liang S (2015) Experimental investigation of residual stress in minimum quantity lubrication grinding of AISI 1018 steel. J Manuf Sci Eng. doi:10.1115/1.4029956

12. Hadad M, Sadeghi B (2012) Thermal analysis of minimum quantity lubrication—MQL grinding process. Int J Mach Tools Manuf 63:1–15. doi:10.1016/j.ijmachtools.2012.07.003

13. Shao Y, Liang S (2014) Predictive force modeling in MQL (mini-mum quantity lubrication) grinding. Proceedings of the ASME 2014 International Manufacturing Science and Engineering Conference, Detroit. doi:10.1115/MSEC2014-3971

14. Shao Y, Li B, Chiang K, Liang S (2015) Physics-based analysis of minimum quantity lubrication grinding. Int J Adv Manuf Technol. doi:10.1007/s00170-015-6941-5

15. McDowell D (1997) Approximate algorithm for elastic–plastic two-dimensional rolling/sliding contact. Wear 211(2):237–246. doi:10.1016/S0043-1648(97)00117-8

16. Kato S, Marui E, Hashimoto M (1998) Fundamental study on nor-mal load dependency of friction characteristics in boundary lubri-cation. Tribol Trans 41(3):341–349. doi:10.1080/10402009808983757

17. Ding Z, Li B, Zou P, Liang S (2014) Material phase transformation during grinding. Adv Mater Res 1052:503–508. doi:10.4028/www.scientific.net/AMR.1052.503

18. Timoshenko S, Goodier J (1970) Theory of elasticity, Internationalth edn. McGraw-Hill, Singapore

19. Saif M, Hui C, Zehnder A (1993) Interface shear stresses induced by non-uniform heating of a film on a substrate. Thin Solid Films 224(2):159–167. doi:10.1016/00406090(93)90427-Q

20. List G, Stter G, Bouthiche A (2012) Cutting temperature prediction in high speed machining by numerical modelling of chip formation and its dependence with crater wear. Int J Mach Tools Manuf 54–55:1–9. doi:10.1016/j.ijmachtools.2011.11.009